Fabrication of Si(111) crystalline thin film on graphene by aluminum-induced crystallization

I. M. Høiaas, D. C. Kim, and H. Weman 🆔

View Online   Export Citation   CrossMark

ARTICLES YOU MAY BE INTERESTED IN

Fabrication of Si(111) crystalline thin film on graphene by aluminum-induced crystallization

I. M. Høiaas,[1] D. C. Kim,[1,2,a)] and H. Weman[1,2,a)]

[1]*Department of Electronics and Telecommunications, Norwegian University of Science and Technology, NO-7491 Trondheim, Norway*
[2]*CrayoNano AS, Otto Nielsens vei 12, NO-7052 Trondheim, Norway*

We report the fabrication of a Si(111) crystalline thin film on graphene by the aluminum-induced crystallization (AIC) process. The AIC process of Si(111) on graphene is shown to be enhanced compared to that on an amorphous SiO_2 substrate, resulting in a more homogeneous Si(111) thin film structure as revealed by X-ray diffraction and atomic force microscopy measurements. Raman measurements confirm that the graphene is intact throughout the process, retaining its characteristic phonon spectrum without any appearance of the D peak. A red-shift of Raman peaks, which is more pronounced for the 2D peak, is observed in graphene after the crystallization process. It is found to correlate with the red-shift of the Si Raman peak, suggesting an epitaxial relationship between graphene and the adsorbed AIC Si(111) film with both the graphene and Si under tensile strain. © 2016 Author(s). All article content, except where otherwise noted, is licensed under a Creative Commons Attribution (CC BY) license (*http://creativecommons.org/licenses/by/4.0/*). [*http://dx.doi.org/10.1063/1.4947101*]

One of the most interesting applications of graphene for future electronic and photonic devices is to integrate it with currently widely used Si and III-V semiconductors in such a way that the characteristic properties of both graphene and semiconductors are well retained and utilized for their high performance. Several pioneering examples can be mentioned, for example, graphene-Si junctions for triode barristors and solar cells,[1,2] and the epitaxial integration of III-V semiconductor nanowires with graphene as a substrate.[3,4]

On combining graphene with Si, most studies are focused on devices where commercially available crystalline Si substrates are used with transferred graphene on top. The opposite case, using graphene as a substrate and depositing Si on top of graphene, is rarely reported.[5–7] In fact, graphene is considered to be chemically inert due to its lack of dangling bonds, resulting in a low adsorption probability of foreign atoms and molecules. It has been found that graphene retains its high quality by direct deposition of Si[7] and its sheet resistance when covered with a thin Si capping layer after post-crystallization,[5] due to the reduced carrier mobility being compensated by an increase in carrier concentration. If the crystal quality of the Si layer can be improved, the conductance of the Si/graphene film may be further increased.

In this letter, we present a method that allows for a crystalline (111)-oriented Si thin film on graphene as a substrate by a crystallization process of Si termed metal-induced crystallization (MIC). Using Al as the metal (AIC), this process is known to give a high quality Si film with a large grain size.[8] By combining this with transparent and flexible graphene, it can be highly beneficial for low cost production of Si photovoltaic cells[9,10] and photodetectors[11] as well as for the epitaxial growth of III-V nanowire devices on graphene.[12] The latter

requires an (111)-orientation of the Si film, and the growth of vertical GaAs nanowires on a 10 nm thick crystallized Si(111) layer on SiO_2 has been demonstrated.[13,14]

MIC is a diffusion-driven process, where thin layers of metal and Si are deposited on top of each other before undergoing an annealing step at 150–500 °C.[15,16] Al and Ni form eutectics with Si and can be used as the metal catalyst.[17,18] The Si diffuses through the metal layer and rearranges as a crystalline film at the metal/substrate interface, making the Si and metal layers exchange positions. The coverage and orientation of the Si are determined by the thickness of the metal and Si layers as well as the annealing process. With Al as the metal layer, the process has been investigated to obtain crystallized Si films on arbitrary substrates[19] with either (001)- or (111)-orientation. Kurosawa *et al.* have summarized which parameters favor which orientation, concluding that longer Al oxidation time and thinner (<100 nm) Al layers result in (111)-oriented Si.[20]

The samples used in this study were of two types processed in parallel: commercial chemical vapor deposition (CVD) grown monolayer graphene transferred onto Si(001) substrates from Graphenea S.A. and thermal SiO_2 (300 nm)/ Si(001) substrates, respectively. The purpose of the latter substrate is to check the overall MIC process with optimized process parameters, in comparison with the substrate with graphene. On these samples, we deposited 50 nm Al by e-beam evaporation at a rate of 1 Å/s and a pressure of $\sim 10^{-8}$ Torr. The samples were oxidized for 24 h in an ISO5 cleanroom atmosphere before depositing 50 nm amorphous Si (a-Si) by e-beam evaporation at a rate of 1 Å/s and a pressure of $\sim 10^{-8}$ Torr. All depositions were done at room temperature. The samples were annealed for 15 h at 500 °C in a nitrogen gas. This temperature was chosen to decrease the annealing time as much as possible while still staying well below the Al-Si eutectic temperature of 577 °C. After the layer exchange by annealing, the top layer of Al was removed by etching in a

---

a)Authors to whom correspondence should be addressed. Electronic addresses: dc.kim@crayonano.com and helge.weman@ntnu.no

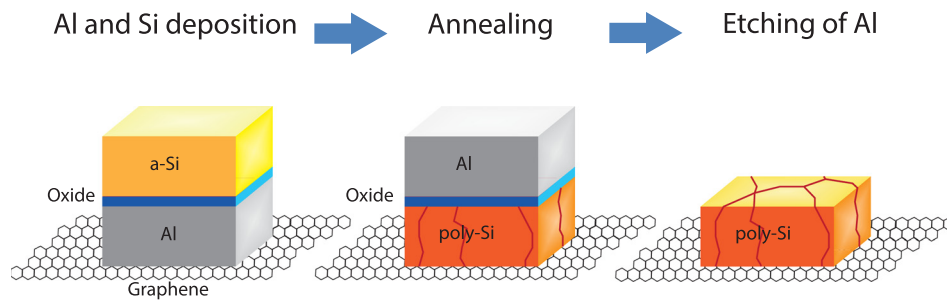Al and Si deposition   Annealing   Etching of Al

FIG. 1. Schematic showing the process steps of the Al-induced crystallization (AIC) process on graphene. An Al layer is first deposited and subsequently oxidized at room temperature for 24 h. Amorphous silicon (a-Si) is deposited on top of the stack, and the whole structure is annealed in a N_2 atmosphere. The layers exchange positions as the Si atoms diffuse towards the substrate and rearrange as a polycrystalline Si film (poly-Si), and the top layer of Al can be etched away.

phosphoric acid mixture.[21] The overall process is shown in Figure 1. X-ray diffraction (XRD) measurements were done with a D8 HRXRD system, and the data shown here have been normalized to the Si(004) substrate peak intensity. Atomic force microscopy (AFM) images were acquired with a Veeco Multimode V system. The Raman spectra were collected by a Renishaw micro-Raman backscattering spectroscopy system using a 532 nm focused laser beam and 50× objective lens. Raman maps were created by collecting spectra with a step size of 1 μm from a 20 μm × 20 μm area. Average peak positions and peak widths were calculated by averaging the values of 25 random spectra from the map.

It is worth to note that there is one major difference in our aluminum-induced crystallization (AIC) process compared to the conventional process. Most groups investigating the AIC process use sputtering for the Al layer deposition, which gives a preferable (111)-orientation of the Al grains.[22] However, the sputtering process involving a plasma with high-energy particles may damage the graphene layer, whereas e-beam evaporation provides a more gentle approach. In our experience, it is imperative to have a high vacuum during the e-beam Al deposition step. If the vacuum is too low ($>10^{-7}$ Torr), the layer exchange between Si and Al is incomplete, resulting in poor Si(111) crystallization. We suspect this might be because the microstructure of Al is affected by the deposition pressure. Further investigations are needed to check this hypothesis.

The XRD data shown in Figure 2 were taken after e-beam deposition of Al and amorphous Si (top graph),

after annealing (middle graph) and after etching of the top Al layer (bottom graph) on the graphene/Si(100) and SiO_2(300 nm)/Si(100) substrates. From Figure 2, it is observed that the as-deposited Al film is different for the two substrates. While all the Al(111)-, Al(002)-, and Al(022)-peaks show approximately the same intensity for the SiO_2 sample, the Al(111) peak is about ten times as large as the other crystal orientations for the graphene sample. Furthermore, the Si(111) peak that appears after annealing is more than ten times larger than the Al(111) peak for the graphene sample, while it is only twice as large compared to the largest Al-peak for the SiO_2-sample. The data imply that the graphene directly affects the film formation of Al and consequently the AIC process. It should be mentioned here that the effect of the Si(100) substrate below graphene on the observed enhanced AIC process should be negligible. The Si(100) substrate was exposed to air before the graphene transfer so it is covered with a native amorphous oxide, similar to the SiO_2/Si(001) substrate. The prominent Al(111) peak may be explained in terms of an epitaxial relationship with graphene. The triangular lattice of the Al(111) plane matches well with the hexagonal lattice structure of graphene with a lattice mismatch of 0.8%, while the other (002) and (022) Al planes have a lattice mismatch of more than 10%.[23] The Al(002)- and Al(022) reflections can still be observed after etching, and we attribute this to local Al residues in some areas of the sample. These local residues could potentially be detrimental to device performance, and further improvement of the Al removal might be necessary.

Optical microscopy and AFM images of the two samples processed in parallel are shown in Figure 3. The appearance of the Si films differs both due to the color of the underlying substrate and their morphology after the AIC process. Dendrite structures are clearly visible in the images of the SiO_2 sample, which are not observed on the graphene sample. The height profiles in the AFM images (Figs. 3(e) and 3(f)) show that there are two distinct layers present on the SiO_2 sample which are not observed on the graphene sample. The dendrites seen in the optical images are islands with a height of about 30 nm on top of a 50 nm layer, which corresponds to the original Al thickness. The islands observed in Figures 3(a) and 3(c) are similar to what is observed for the crystallization process of Ge,[24] showing two distinct layers corresponding to the original thickness of Al and a-Si of 50 nm. Figure 3 indicates that the Si(111) film obtained by AIC on graphene is smoother than that obtained
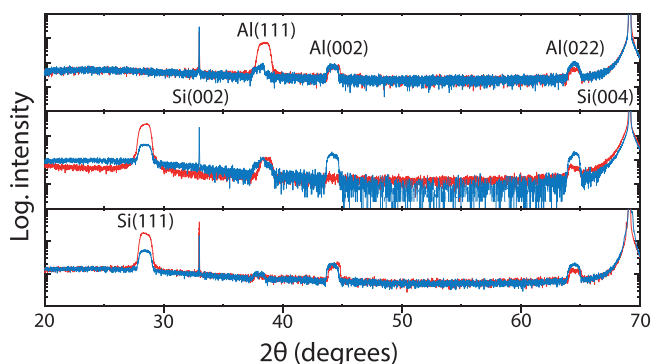
FIG. 2. XRD $2\theta/\omega$ scans after deposition of Al and amorphous Si (top), after the Al-induced crystallization of Si (middle), and after the etching of Al (bottom). The red scans are from the graphene/Si(100) sample and the blue scans are from the SiO_2/Si(100) sample. The data have been normalized to the intensity of the substrate Si(004) peak. The Si(002) peak is also from the Si substrate.
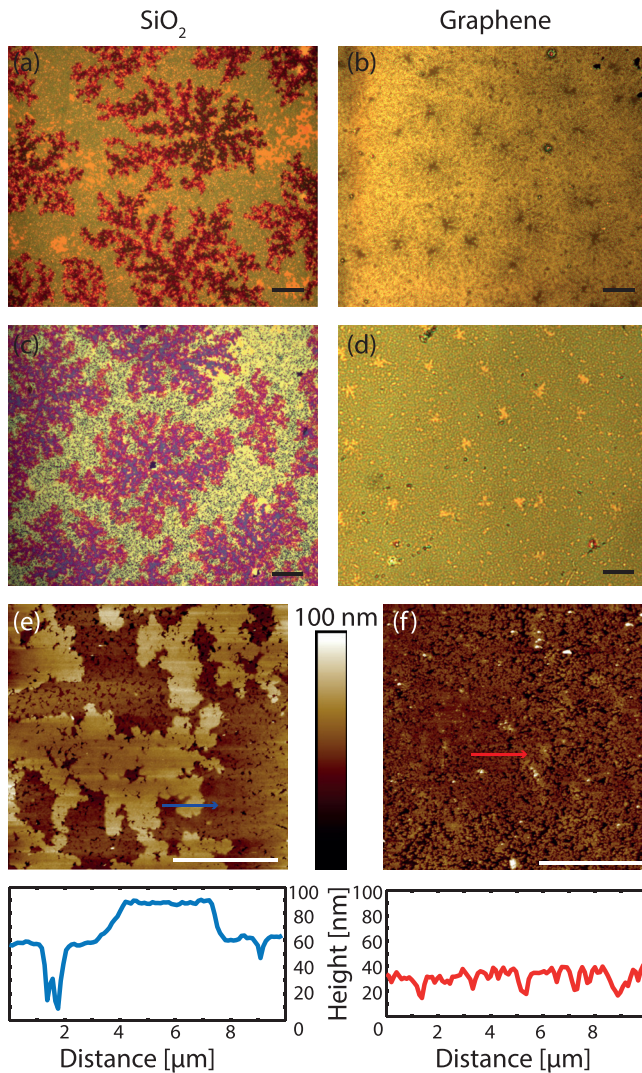
SiO$_2$ Graphene

FIG. 3. Optical images show the SiO$_2$ sample (a) after the Al-induced crystallization process and (c) after subsequent Al etching, and the graphene sample (b) after the Al-induced crystallization and (d) after subsequent Al etching. AFM images of (e) the SiO$_2$ sample and (f) the graphene sample. AFM line scans from (e) and (f) (denoted by blue and red arrows, respectively) are shown in the bottom panels. All scale bars are 20 μm.

by AIC on SiO$_2$ with more homogeneity in thickness. Some local Al residues can be seen as bright spots in Figure 3(d).

It is already known that the substrate can influence the crystallization of Si. Toko *et al.* concluded that the type of substrate was important for the resulting Si-orientation, but could not determine the exact origin except for excluding the roughness of the substrate for being the reason.[19] They suggested that the difference in interfacial energy between Si and the substrate is the determining factor, but not in what form. The two samples used in this report for the AIC process: a graphene/Si(001) substrate and a SiO$_2$/Si(001) substrate, respectively, were processed in parallel, so the difference observed in the crystallized Si film should be a direct effect of the substrate properties.

The AIC processed Al/Si layer on top of graphene can be easily exfoliated from the Si(100) substrates by using scotch tape as shown in Figure 4(a). This indicates that the interaction between the AIC processed Si layer and graphene gives stronger adhesion than the usual van der Waals interaction between graphene and the bottom Si(001) substrate, and

that the AIC process occurs on the graphene surface without any chemical interaction with the Si(100) substrate.

Figures 4(b)–4(e) show the Raman spectra and Raman mapping data of crystallized Si and graphene measured after exfoliation. The absence of the D peak at $\sim$1320 cm^{-1} in the graphene spectra indicates that the AIC process does not damage the graphene, similar to other results from Si deposited on graphene devices.[5,7] Compared to the reference Si peak from a standard Si(100) substrate (520 cm^{-1}) and graphene peaks from bare CVD graphene (G peak at 1591 cm^{-1}, 2D peak at $\sim$2684 cm^{-1}) on Si substrates, the AIC processed Si and graphene show red-shifts of the Raman peaks. The Raman mapping reveals that the red-shifts of the Si and graphene Raman peaks are correlated; the regions experiencing the largest red-shift of the Si peak also experience the largest red-shift of the graphene peaks. The red-shift is more prominent for the 2D peak, which shifts up to $\sim$24 cm^{-1}. This observation is opposite to previous results from e-beam crystallized Si on graphene, and Si-islands deposited on graphene where blue-shifts of both the G and 2D peaks were observed.[5,6]

A shift of the characteristic phonon modes of graphene indicates a change in doping and/or strain in the graphene layer. In a comprehensive study, Das *et al.* showed that field-effect doping of graphene leads to a blue-shift of the G peak and a red- or blue-shift of the 2D peak depending on the charge of the doping.[25] The simultaneous red-shift of the G and 2D peak indicates that tensile strain in graphene is the origin of the shift. The Al-induced crystallized Si has been known to be heavily p-doped by Al impurity atoms with values $\sim$10^{18}–10^{19} atoms/cm^3.[26–28] This could give rise to p-doping in graphene. According to the correlation analysis of the G and 2D peak positions by Lee *et al.*, the effects of strain and doping can be separated. From the average values of the G and 2D peak positions in Table I of 1584.5 cm^{-1} and 2669.3 cm^{-1}, respectively, the graphene with the AIC processed Si(111) film has a tensile strain of $\sim$0.25% and a hole doping concentration of $\sim$7 $\times$ 10^{12} cm^{-2}.[29]

The red-shift of the Si peak at 520 cm^{-1} indicates that a tensile strain is present also in the crystallized Si(111) thin film. The correlation of the red-shift of the Si peak with that of the graphene peaks indicates some form of chemical bonding between the crystallized Si and graphene. We therefore next consider the possible adsorption sites of Si atoms in the (111) plane on graphene that would give rise to an epitaxial chemical binding. Theoretical calculations of the adsorption of a single Si adatom on three different graphene sites—H-sites: hollow sites above the centers of C hexagons, T-sites: sites on top of C atoms, and B-sites: bridge sites above the midpoints of C-C bonds—on graphene predict that the B-site is the most stable absorption site, followed by the T-site with a slight decrease of the adsorption energy of less than 0.1 eV. The H-site is the least favorable one with an adsorption energy difference of more than 0.4 eV.[30,31] However, for Si atoms in a (111) lattice plane which have one dangling bond, it is quite different. First-principles calculations show similar adsorption energy in all three site configurations.[32] Figure 5 shows possible arrangements of Si atoms in a (111)-plane above the hexagonal graphene lattice with the Si atoms at B-, T-, and H-sites. Figures 5(a) and 5(b) show the configuration when the center Si atom is adsorbed at the B-and T-site,
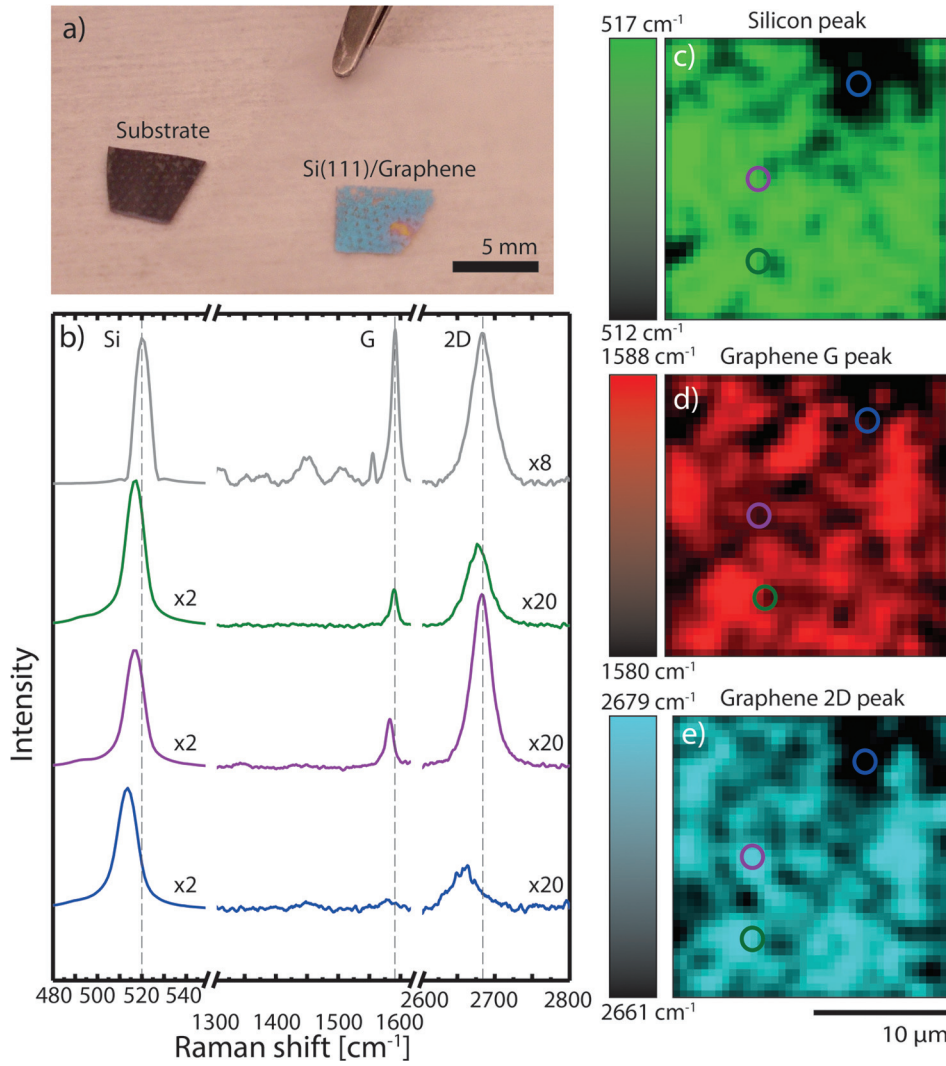
FIG. 4. (a) Photograph of the AIC processed Si(111)/graphene sample after exfoliation from the Si(001) substrate. (b) Raman spectra from the crystallized Si and graphene after the AIC process. Raman mapping images corresponding to (c) the position of the Si peak, (d) the graphene G peak, and (e) the graphene 2D peak. In (b), spectra from random locations denoted by circles in (c), (d), and (e) are shown together with a reference spectrum from pristine graphene on a Si(100) substrate (top). The peak positions of the reference spectrum are indicated with vertical dashed lines. The heights of the Si peaks and the graphene reference peaks have been normalized to fit the plot.

respectively, with a Si interatomic distance (a_{Si-Si}) between the relaxed Si atoms (blue solid circles) of 3.840 Å. The green hexagon in Figure 5(a) represents a lattice-matched arrangement of atoms in a (111)-plane on graphene with an interatomic distance $a = 3.694$ Å. The red hexagon in Figure 5(b) represents a lattice-matched arrangement of atoms in a (111)-plane on graphene with an interatomic distance $a = 3.762$ Å. The same green and red hexagonal arrangements can also be obtained for the case when the center Si atom is adsorbed at the H-site (Fig. 5(c)). The lattice mismatch between (relaxed) Si(111) and graphene with the green and red hexagonal configurations is 3.95% and 2.07%, respectively. If conventional

epitaxial growth of Si(111) on graphene is considered, graphene would be tensile strained while Si would be compressively strained as a is smaller than a_{Si-Si}. However, in the Raman data (Fig. 4) tensile strain in the AIC crystallized Si on graphene is observed. The MIC process itself is known to introduce stress in the Si film, and this stress can be either compressive or tensile depending on the process conditions.[33,34] It is worth to note here that we also observe a redshift of the Si Raman peak of the AIC Si on SiO$_2$ in this study. Therefore, if one considers that the crystal structure of Si is (111)-oriented with tensile strain from the AIC process, it appears that graphene adapts to the tensile strained Si to meet the epitaxial relationship.

Theoretical calculations on the adsorption of single Si atoms or a (111) plane of Si atoms on graphene predict a strong chemisorption forming Si-C covalent bonds.[30–32] This will affect the electronic structure of graphene significantly, and even induce a large band gap in graphene.[32] In addition, there is disagreement to whether strain in graphene opens up a band-gap or not.[35,36] Since the Si/graphene interface in our samples is formed from the Si-Al interchange at an elevated temperature, Si(111) and graphene may form a clean junction, which is not possible if graphene is transferred on top of Si.

In summary, a heterostructure comprised of CVD graphene and crystallized Si(111) has been fabricated by an

TABLE I. Values for the mean frequency $\bar{\nu}$ and full width at half maximum (FWHM) of Si and graphene main Raman peaks from the positions shown in the map in Figure 4 for graphene with crystallized Si(111) on top. Values from Si(001)/G are reference values obtained from CVD graphene transferred to a Si(001) substrate.

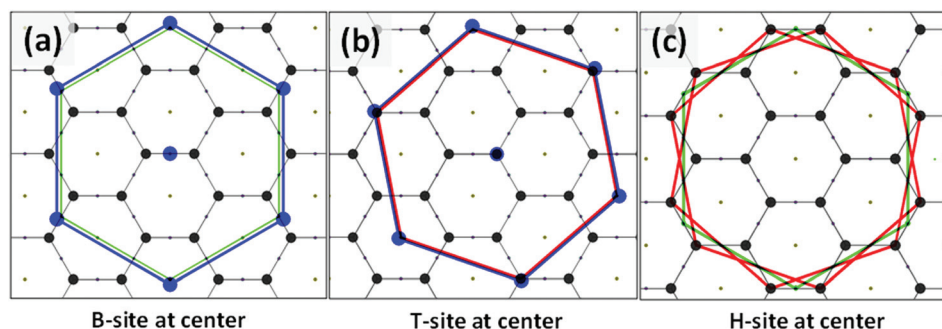|	$\bar{\nu}_{Si}$ (cm^{-1})	FWHM$_{Si}$ (cm^{-1})	$\bar{\nu}_{G}$ (cm^{-1})	FWHM$_{G}$ (cm^{-1})	$\bar{\nu}_{2D}$ (cm^{-1})	FWHM$_{2D}$ (cm^{-1})
Si(001)/G	520.3	7.4	1591.0	13.1	2683.6	36.2
Blue position	513.4	10.8	1579.8	27.5	2659.6	42.4
Purple position	516.7	9.7	1582.6	14.5	2682.3	31.6
Green position	516.9	9.6	1589.5	12.1	2677.7	36.9
Average	515.7	8.6	1584.5	14.4	2669.3	37.1

FIG. 5. Epitaxial arrangements of atoms in the (111) plane on top of the hexagonal graphene lattice. Large black solid circles denote the C atoms, which also correspond to the T-site configuration. B- and H-site configurations are denoted as small solid gray circles in the graphene lattice. In (a) and (b), the blue solid circles denote Si atoms with the blue hexagons indicating the (relaxed) Si atomic arrangement in the (111) plane with a Si-Si interatomic distance, a_{Si-Si}, of 3.840 Å. Three epitaxial configuration cases are shown: when the center Si atom is adsorbed at the (a) B-site, (b) T-site, and (c) H-site. The green hexagons in (a) and (c) represent lattice-matched arrangements of atoms in a Si(111) plane on graphene with an interatomic distance $a = 3.694$ Å. The red hexagons in (b) and (c) represent lattice-matched arrangement of atoms in a Si(111) plane on graphene with $a = 3.762$ Å. There are two possible lattice-matched arrangements for the red hexagonal configurations for the H-site at center case in (c).

AIC process. Improvement of crystallization and homogeneity of the Si(111) thin film has been observed with graphene compared to SiO$_2$ samples. Red-shifts in the Raman G and 2D peak positions indicate a tensile strain in the graphene. The red-shifts of the graphene Raman peaks correlate with a red-shift of the Si Raman peak, suggesting an epitaxial relationship with also the crystallized Si(111) under tensile strain. Theoretical modeling show that the adsorption of Si atoms in the (111) plane on graphene can be configured with a lattice mismatch of ∼2%.

[1]H. Yang, J. Heo, S. Park, H. J. Song, D. H. Seo, K. Byun, P. Kim, I. Yoo, H. Chung, and K. Kim, Science **336**, 1140 (2012).
[2]X. Miao, S. Tongay, M. K. Petterson, K. Berke, A. G. Rinzler, B. R. Appleton, and A. F. Hebard, Nano Lett. **12**, 2745 (2012).
[3]A. M. Munshi, D. L. Dheeraj, V. T. Fauske, D. C. Kim, A. T. J. Van Helvoort, B. O. Fimland, and H. Weman, Nano Lett. **12**, 4570 (2012).
[4]Y. J. Hong and T. Fukui, ACS Nano **5**, 7576 (2011).
[5]M. A. Gluba, D. Amkreutz, G. V. Troppenz, J. Rappich, and N. H. Nickel, Appl. Phys. Lett. **103**, 073102 (2013).
[6]D. H. Lee, J. Yi, J. M. Lee, S. J. Lee, Y. J. Doh, H. Y. Jeong, Z. Lee, U. Paik, J. A. Rogers, and W. Il Park, ACS Nano **7**, 301 (2013).
[7]G. Lupina, J. Kitzmann, M. Lukosius, J. Dabrowski, A. Wolff, and W. Mehr, Appl. Phys. Lett. **103**, 263101 (2013).
[8]M. Kurosawa, N. Kawabata, T. Sadoh, and M. Miyao, Appl. Phys. Lett. **95**, 132103 (2009).
[9]F. Delachat, F. Antoni, P. Prathap, A. Slaoui, C. Cayron, and C. Ducros, EPJ Photovoltaics **4**, 45102 (2013).
[10]D. Tsukada, Y. Matsumoto, R. Sasaki, M. Takeishi, T. Saito, N. Usami, and T. Suemasu, J. Cryst. Growth **311**, 3581 (2009).
[11]X. Li, M. Zhu, M. Du, Z. Lv, L. Zhang, Y. Li, Y. Yang, T. Yang, X. Li, K. Wang, H. Zhu, and Y. Fang, Small **12**, 595 (2015).
[12]M. Munshi and H. Weman, Phys. Status Solidi RRL. **7**, 713 (2013).
[13]Y. Cohin, O. Mauguin, L. Largeau, G. Patriarche, F. Glas, E. Søndergård, and J. C. Harmand, Nano Lett. **13**, 2743 (2013).
[14]D. Ren, I. M. Høiaas, J. F. Reinertsen, D. L. Dheeraj, A. M. Munshi, D. C. Kim, H. Weman, and B. O. Fimland, J. Vac. Sci. Technol. B **34**, 02L117 (2016).
[15]M. Shahidul Haque, H. A. Naseem, and W. D. Brown, J. Appl. Phys. **75**, 3928 (1994).
[16]T. J. Konno and R. Sinclair, Mater. Sci. Eng. A **179–180**, 426 (1994).
[17]O. Nast, T. Puzzer, L. M. Koschier, A. B. Sproul, and S. R. Wenham, Appl. Phys. Lett. **73**, 3214 (1998).
[18]S. Y. Yoon, S. J. Park, K. H. Kim, J. Jang, and C. O. Kim, J. Appl. Phys. **87**, 609 (2000).
[19]K. Toko, M. Nakata, A. Okada, M. Sasase, N. Usami, and T. Suemasu, Int. J. Photoenergy **2015**, 790242.
[20]M. Kurosawa, T. Sadoh, and M. Miyao, J. Appl. Phys. **116**, 173510 (2014).
[21]K. R. Williams and R. S. Muller, J. Microelectromech. Syst. **5**, 256 (1996).
[22]A. Lita and J. Sanchez, J. Appl. Phys. **85**, 876 (1999).
[23]C. Gong, G. Lee, B. Shan, E. M. Vogel, R. M. Wallace, and K. Cho, J. Appl. Phys. **108**, 123711 (2010).
[24]K. Toko, K. Nakazawa, N. Saitoh, N. Yoshizawa, and T. Suemasu, Cryst. Growth Des. **15**, 1535 (2015).
[25]A. Das, S. Pisana, B. Chakraborty, S. Piscanec, S. K. Saha, U. V. Waghmare, K. S. Novoselov, H. R. Krishnamurthy, A. K. Geim, A. C. Ferrari, and A. K. Sood, Nat. Nanotechnol. **3**, 210 (2008).
[26]I. Gordon, D. Van Gestel, K. Van Nieuwenhuysen, L. Carnel, G. Beaucarne, and J. Poortmans, Thin Solid Films **487**, 113 (2005).
[27]O. Nast and S. R. Wenham, J. Appl. Phys. **88**, 124 (2000).
[28]O. Nast and A. J. Hartmann, J. Appl. Phys. **88**, 716 (2000).
[29]J. E. Lee, G. Ahn, J. Shim, Y. S. Lee, and S. Ryu, Nat. Commun. **3**, 1024 (2012).
[30]C. H. Hu, Y. Zheng, Y. Zhang, S. Q. Wu, Y. H. Wen, and Z. Z. Zhu, Solid State Commun. **151**, 1128 (2011).
[31]E. Aktürk, C. Ataca, and S. Ciraci, Appl. Phys. Lett. **96**, 123112 (2010).
[32]X. Dang, H. Dong, L. Wang, Y. Zhao, T. Guo, T. Hou, Y. Li, and S. Lee, ACS Nano **9**, 8562 (2015).
[33]T. N. Nguyen, V. D. Nguyen, S. Jung, and J. Yi, Microelectron. Eng. **87**, 2163 (2010).
[34]C. C. Peng, C. K. Chung, and J. F. Lin, Acta Mater. **59**, 6093 (2011).
[35]T. M. G. Mohiuddin, A. Lombardo, R. R. Nair, A. Bonetti, G. Savini, R. Jalil, N. Bonini, D. M. Basko, C. Galiotis, N. Marzari, K. S. Novoselov, A. K. Geim, and A. C. Ferrari, Phys. Rev. B **79**, 205433 (2009).
[36]Z. H. Ni, T. Yu, Y. H. Lu, Y. Y. Wang, Y. P. Feng, and Z. X. Shen, ACS Nano **2**, 2301 (2008).